

A NON-CONVEX OPTIMIZATION TECHNIQUE FOR SPARSE BLIND DECONVOLUTION – INITIALIZATION ASPECTS AND ERROR REDUCTION PROPERTIES

ANIRUDDHA ADIGA* AND CHANDRA SEKHAR SEELAMANTULA*

Abstract. Sparse blind deconvolution is the problem of estimating the blur kernel and sparse excitation, both of which are unknown. Considering a linear convolution model, as opposed to the standard circular convolution model, we derive a sufficient condition for stable deconvolution. The columns of the linear convolution matrix form a Riesz basis with the tightness of the Riesz bounds determined by the autocorrelation of the blur kernel. Employing a Bayesian framework results in a non-convex, non-smooth cost function consisting of an ℓ_2 data-fidelity term and a sparsity promoting ℓ_p -norm ($0 \leq p \leq 1$) regularizer. Since the ℓ_p -norm is not differentiable at the origin, we employ an ϵ -regularized ℓ_p -norm as a surrogate. The data term is also non-convex in both the blur kernel and excitation. An iterative scheme termed alternating minimization (Alt. Min.) $\ell_p - \ell_2$ projections algorithm (ALPA) is developed for optimization of the ϵ -regularized cost function. Further, we demonstrate that, in every iteration, the ϵ -regularized cost function is non-increasing and more importantly, bounds the original ℓ_p -norm-based cost. Due to non-convexity of the cost, the accuracy of estimation is largely influenced by the initialization. Considering regularized least-squares estimate as the initialization, we analyze how the initialization errors are concentrated, first in Gaussian noise, and then in bounded noise, the latter case resulting in tighter bounds. Comparisons with state-of-the-art blind deconvolution algorithms show that the deconvolution accuracy is higher in case of ALPA. In the context of natural speech signals, ALPA results in accurate deconvolution of a voiced speech segment into a sparse excitation and smooth vocal tract response.

Key words. Sparse blind deconvolution, non-convex optimization, alternating minimization, majorization-minimization, blind deconvolution of speech signals, concentration inequalities.

AMS subject classifications. 65F22, 65F10, 49N45

1. Introduction.

$$(1) \quad \mathbf{y} = \mathbf{h} * \mathbf{e} + \mathbf{w},$$

where $*$ denotes linear convolution, the observation $\mathbf{y} \in \mathbb{R}^N$, the blur kernel $\mathbf{h} \in \mathbb{R}^L$, the excitation $\mathbf{e} \in \mathbb{R}^M$, the acquisition noise $\mathbf{w} \in \mathbb{R}^N$, and $N = L + M - 1$. Such linear shift-invariant (LSI) models are frequently encountered in geophysics [53], speech processing [39, 45], image processing [33, 36, 42], etc. In microscopy [52], astronomy [42], and photography applications, etc., the vector \mathbf{h} denotes the point-spread function (the blur kernel) of the imaging system, \mathbf{e} is the underlying sharp image, and \mathbf{y} is the blurred captured image. The blur kernel accounts for finite aperture of the imaging system, possible camera motion, defocus, atmospheric disturbances, etc. In a speech processing context, for voiced sounds, \mathbf{h} models the vocal-tract filter response, \mathbf{e} is the quasi-periodic glottal excitation, and \mathbf{y} denotes the sampled speech signal [39].

The goal in blind deconvolution is to estimate \mathbf{h} and \mathbf{e} given \mathbf{y} and the statistics of \mathbf{w} . The problem is inherently ill-posed as there exist infinitely many combinations of \mathbf{h} and \mathbf{e} that give rise to the same \mathbf{y} . Taking into account available priors on \mathbf{h} and \mathbf{e} would constraint the solution space. We consider the widely applicable case of a sparse excitation and a relatively smooth and localized blur kernel. In several applications such as deblurring of star-field images [27, 42], fluorophore localization in super-resolution microscopy [52], source-filter modeling of voiced speech signals [39, 45], separation of the reflectivity function from the source signature in seismic signals [53],

*Department of Electrical Engineering, Indian Institute of Science, Bangalore - 560 012, India (aaniruddha, chandrasekhar@iisc.ac.in).

etc., the excitation is innately sparse, and the blur kernel is a lowpass function. While in some cases, sparsity manifests directly, in others, sparsity becomes apparent only after performing a suitable transformation, for instance, the wavelet transform.

1.1. A Maximum a Posteriori (MAP) Formulation for Sparse Blind Deconvolution. Within a Bayesian setting, the *maximum a posteriori* (MAP) estimates of the filter \mathbf{h} and excitation \mathbf{e} are given by the joint optimization:

$$(2) \quad (\mathbf{h}_{\text{opt}}, \mathbf{e}_{\text{opt}}) = \arg \max_{(\mathbf{h}, \mathbf{e})} g(\mathbf{y}/\mathbf{e}; \mathbf{h})f(\mathbf{e}),$$

where g is the likelihood of the observations and f denotes the prior on \mathbf{e} . Let \mathbf{e} have i.i.d. entries following a *generalized p -Gaussian* (gpG) distribution [27], which results in the prior

$$(3) \quad f(\mathbf{e}) = \left(\frac{p}{2\Gamma(1/p)\gamma\sigma_e} \right)^M \exp \left(- \sum_{i=0}^{M-1} \left(\frac{|e_i|}{\gamma\sigma_e} \right)^p \right),$$

where $\gamma = \left(\frac{\Gamma(1/p)}{\Gamma(3/p)} \right)^{1/2}$, and e_i denotes the i^{th} entry of \mathbf{e} . For $0 \leq p \leq 1$, f is a heavy-tailed distribution that yields sparse sequences [27], which is the scenario of interest in this paper. As $p \rightarrow 0$, the *kurtosis/peakedness* of the distribution increases, and the tail becomes heavier. With the gpG prior (3), the MAP formulation is equivalent to

$$(4) \quad (\mathbf{h}_{\text{opt}}, \mathbf{e}_{\text{opt}}) = \arg \min_{(\mathbf{h}, \mathbf{e})} \|\mathbf{y} - \mathbf{h} * \mathbf{e}\|_2^2 + \frac{2\sigma_w^2}{(\gamma\sigma_e)^p} \|\mathbf{e}\|_p^p,$$

with ℓ_p -norm regularization coming up naturally. In a practical setting, if the distribution parameters are not known, a viable alternative is to solve

$$(5) \quad (\mathbf{h}_{\text{opt}}, \mathbf{e}_{\text{opt}}) = \arg \min_{\mathbf{h}, \mathbf{e}} \underbrace{\|\mathbf{y} - \mathbf{h} * \mathbf{e}\|_2^2 + \delta \|\mathbf{e}\|_p^p}_{F(\mathbf{h}, \mathbf{e})},$$

where δ is the regularization parameter that controls the trade-off between data fidelity and sparsity and could be fixed experimentally or using cross-validation [22].

ℓ_p -quasi-norms, $0 \leq p < 1$, and ℓ_1 -norm are popular sparsity promoting priors and have been employed extensively in the general class of linear inverse problems [4, 27, 34, 46], image deconvolution [27], speech coding [21] and sparse recovery problems [12, 46]. The ℓ_1 -norm is used in the least absolute shrinkage and selection operator (LASSO) [54], basis-pursuit denoising problems [13], and as a convex proxy for the ℓ_0 -quasi-norm in compressed sensing (CS) problems [9]. However, if one were to use the ℓ_p -norm ($0 \leq p < 1$), fewer random projections would be required as compared with the ℓ_1 -norm [11].

As the ℓ_p -norms suffer from local non-differentiability, optimization is carried out using gradient-based iterative solvers [4, 20], majorization-minimization (MM) approaches [26] such as the iteratively reweighted least-squares (IRLS) [12, 16], iteratively reweighted ℓ_1 -norm [10] techniques, etc. Early work on deblurring of star-field images using ℓ_p -norm priors proposed in [27] employed simplex search to optimize the non-convex cost.

1.2. Related Literature. In the computer vision and image processing communities, blind deconvolution is almost synonymous with image deblurring. A vast

amount of literature exists on this topic, which makes it impossible to summarize every contribution. We refer the reader to [33] and [8] for a comprehensive review of blind deconvolution algorithms, most of which are set up within a Bayesian framework. Apart from the MAP formulation, there exist other approaches based on the expectation-maximization (EM) algorithm [19, 29], the variational approach [36, 38], quasi-maximum-likelihood approach [7], ADMM [2], etc. Specific to image deconvolution, Levin et al. showed that the naive MAP approach may lead to degeneracy (resulting in the blurred image itself as the blur kernel, and a Kronecker impulse as the excitation) and developed strategies to overcome it [36]. The gradients in natural images were shown to be heavy-tailed, which were parametrically modeled using Gaussian mixtures [18], second-order polynomials [50], non-identical but independent Gaussians [57], etc.

Non-parametric regularizers include the ℓ_p -norm [28, 31, 35], the ℓ_1/ℓ_2 [32, 47], the isotropic total-variation (TV) regularizer [43, 56], and the p^{th} power TV norm [30]. The ℓ_p -norm-based cost function is optimized using IRLS [28, 35] or using separable regularizers [31]. The ℓ_1 -norm is influenced by the amplitudes of the estimates and may not always yield a sparse solution. In order to circumvent this problem, the scale-invariant ℓ_1/ℓ_2 function was considered in [32], and a LASSO solver is used to optimize the cost by rescaling with the ℓ_2 -norm from the previous iteration. Repetti *et al.* [47] developed an approach consisting of a combination of MM and proximal methods to optimize a smoothed ℓ_1/ℓ_2 regularized cost function for blind deconvolution of seismic signals.

Wipf and Zhang [57] solved the image deblurring problem using a variational Bayesian strategy and concave sparsity priors with the degree of concavity adapted to the noise and energy of the blur kernel. Zhang *et al.* [58] considered the multiple measurement counterpart of this problem and showed that a single, low-noise, less blurred observation dominates the multi-observation regularizer and makes it concave. A relatively new class of approaches reformulate the blind deconvolution problem as a low-rank matrix recovery problem from linear measurements, with constraints on the subspace dimension and sparsity to ensure uniqueness, and employ convex programming techniques for recovery [1, 14, 15, 37].

Since we are dealing with a non-convex problem in general, which calls for iterative techniques, the issue of initialization becomes important, mainly from the viewpoint of avoiding local minima. In this paper, we consider the regularized least-squares (reg. LS) estimate as the initialization and analyze concentration of the error from the ground truth.

1.3. Our Contributions. We provide a sufficiency condition for stable deconvolution for the specific case of linear convolution (Proposition 2.1, Section 2). Since the cost function is non-convex and non-smooth, we develop an alternating ℓ_p - ℓ_2 projections algorithm (ALPA) (Section 3) considering a smoothed version of the cost. Further, we show that the iterative algorithm ensures that the smoothed cost is non-increasing in every iteration and upper bounds the original cost function (Section 4, Proposition 4.1). We then consider reg. LS estimate of the excitation as the initialization for ALPA and analyze the concentration of the mean-absolute error of this estimate from the ground truth (Section 5). The error bounds depend on the condition number of the linear system, the regularization parameter, error in filter estimation, and the noise variance (Proposition 5.1). Further, if the noise is bounded, the tail bounds can be made tighter thanks to the Hoeffding inequality (Proposition 5.2). On the application front, we demonstrate successful blind deconvolution of voiced speech signals into a

sparse excitation and vocal-tract filter and compare the results with state-of-the-art techniques (Section 6).

2. A Sufficient Condition for Stable Deconvolution. Consider the matrix form of the linear measurement model in (1):

$$(6) \quad \mathbf{y} = \mathbf{H}\mathbf{e} + \mathbf{w} = \mathbf{E}\mathbf{h} + \mathbf{w},$$

where $\mathbf{E} \in \mathbb{R}^{N \times L}$ and $\mathbf{H} \in \mathbb{R}^{N \times M}$ are linear convolution matrices (cf. (30) in Appendix A) constructed from $\mathbf{e} \in \mathbb{R}^M$ and $\mathbf{h} \in \mathbb{R}^L$, respectively, and the noise vector $\mathbf{w} \sim \mathcal{N}(\mathbf{0}, \sigma_w^2 \mathbf{I})$. The vector \mathbf{h} is assumed to be deterministic. The linear convolution model (6) is a more realistic representation of practical linear, shift-invariant systems than the commonly assumed circular convolution model. Further, it does not lead to degenerate solutions (such as $\mathbf{h}_n = \mathbf{y}_n$ and $\mathbf{e}_n = \delta[n]$, where n denotes the element index, and $\delta[n]$ is the Kronecker impulse, which is the global optimum [5, 36]) that may be encountered in a circular convolution model, because the filter, excitation, and measurement vectors reside in different dimensional spaces.

LEMMA 2.1. *Let $\mathbf{H} \in \mathbb{R}^{N \times M}$ be a linear convolution matrix with columns \mathbf{h}_s , $0 \leq s \leq M - 1$, obtained as shifted versions of the filter \mathbf{h} . Then the set $\{\mathbf{h}_s\}_{s=0}^{L-1}$ forms a Riesz basis with Riesz bounds given as*

$$(7) \quad 0 < \sigma_{\min}^2(\mathbf{H}) \leq \frac{\|\mathbf{H}\mathbf{x}\|_2^2}{\|\mathbf{x}\|_2^2} \leq \sigma_{\max}^2(\mathbf{H}), \quad \forall \mathbf{x} \in \mathbb{R}^M - \{\mathbf{0}\},$$

where $\sigma_{\min}(\mathbf{H})$ and $\sigma_{\max}(\mathbf{H})$ denote the minimum and maximum singular values of \mathbf{H} , respectively.

The proof is given in Appendix A.

It is easy to verify that the columns of \mathbf{H} are linearly independent and hence, the problem of determining \mathbf{e} from \mathbf{y} given \mathbf{h} is *well-posed*, that is, if a solution exists, it would be unique, and a continuous function of the measurements [55]. The conditioning of the system is determined by the tightness of the Riesz bounds.

PROPOSITION 2.1. *Consider a filter \mathbf{h} with $\|\mathbf{h}\|_2 = 1$. Let \mathbf{H} and $r_{\mathbf{h}\mathbf{h}}$ be the corresponding linear convolution matrix and Gram sequence, respectively. The Riesz bases constituted by the columns of \mathbf{H} will have a lower Riesz bound $\sigma_{\min}^2(\mathbf{H}) \geq \eta$ and an upper Riesz bound $\sigma_{\max}^2(\mathbf{H}) \leq 2 - \eta$, where $\eta \in (0, 1]$, if*

$$(8) \quad 0 \leq \sum_{\ell=1}^{(M-1)/2} |r_{\mathbf{h}\mathbf{h}}(\ell)| \leq \frac{1 - \eta}{2}.$$

The proof is given in Appendix B.

The condition number of $\mathbf{H}^T \mathbf{H}$ varies as $1/\eta$. As $\eta \rightarrow 1$, the Riesz bounds become tighter, and the columns of $\mathbf{H}^T \mathbf{H}$ will tend to become orthonormal. A similar sufficiency condition can be derived on the excitation sequence considering the model: $\mathbf{y} = \mathbf{E}\mathbf{h} + \mathbf{w}$. In particular, for periodic and sparse excitation sequences, the Riesz bounds could be tight as illustrated next. For instance, consider the unit-norm periodic sparse excitation $e(n) = \sum_{k=0}^{K-1} a_k \delta(n - kT)$. A filter \mathbf{h} of length T yields a convolution matrix \mathbf{E} with orthonormal columns and hence the autocorrelation of the excitation satisfies: $\sum_{\ell=1}^{(L-1)/2} |r_{\mathbf{e}\mathbf{e}}(\ell)| = 0$. In this instance, since $\mathbf{E}^T \mathbf{E} = \mathbf{I}_{T \times T}$, we have that $\sigma_{\min}^2(\mathbf{E}) = \sigma_{\max}^2(\mathbf{E}) = 1$.

3. The Alternating $\ell_p - \ell_2$ Projections Algorithm. We adopt an *alternating minimization* (Alt. Min.) strategy to solve the optimization problem in (5). In the first step, we fix \mathbf{h} , and optimize $F(\mathbf{h}, \mathbf{e})$ over \mathbf{e} (excitation optimization or *e-step*). In the next step, $F(\mathbf{h}, \mathbf{e})$ is updated with the estimate of \mathbf{e} and then optimized over \mathbf{h} (filter optimization or *h-step*). The Alt. Min. iterations are carried out until a suitable convergence criterion is met.

Let $\mathbf{h}^{(k)}$ denote the filter estimate obtained at the end of the k^{th} iteration. In the *e-step*, $F(\mathbf{h}^{(k)}, \mathbf{e})$ is optimized with respect to \mathbf{e} to obtain $\mathbf{e}^{(k+1)}$:

$$(9) \quad \mathbf{e}^{(k+1)} = \arg \min_{\mathbf{e}} \underbrace{\|\mathbf{y} - \mathbf{H}^{(k)}\mathbf{e}\|_2^2 + \delta\|\mathbf{e}\|_p^p}_{F(\mathbf{h}^{(k)}, \mathbf{e})},$$

where $\mathbf{H}^{(k)} \in \mathbb{R}^{N \times M}$ is a linear convolution matrix constructed from $\mathbf{h}^{(k)}$. For $0 \leq p < 1$, $F(\mathbf{h}^{(k)}, \mathbf{e})$ is non-convex and its gradient with respect to \mathbf{e} , denoted by $\nabla_{\mathbf{e}} F(\mathbf{h}^{(k)}, \mathbf{e})$ has a discontinuity at $\mathbf{e} = \mathbf{0}$. To circumvent the discontinuity, we approximate the ℓ_p -norm with its ϵ -regularized version: $\|\mathbf{e}\|_{p, \epsilon}^p = \sum_{i=0}^{M-1} (e_i^2 + \epsilon)^{p/2}$, $\epsilon > 0$, resulting in the modified cost F_{ϵ} given by

$$(10) \quad F_{\epsilon}(\mathbf{h}^{(k)}, \mathbf{e}) = \|\mathbf{y} - \mathbf{H}^{(k)}\mathbf{e}\|_2^2 + \delta\|\mathbf{e}\|_{p, \epsilon}^p.$$

Replacing $F(\mathbf{h}^{(k)}, \mathbf{e})$ in (9) with $F_{\epsilon}(\mathbf{h}^{(k)}, \mathbf{e})$, the estimate of \mathbf{e} in the $(k+1)^{\text{st}}$ iteration is obtained as follows:

$$\mathbf{e}^{(k+1)} = \arg \min_{\mathbf{e}} F_{\epsilon}(\mathbf{h}^{(k)}, \mathbf{e}).$$

The cost function $F_{\epsilon}(\mathbf{h}^{(k)}, \mathbf{e})$ is differentiable with respect to \mathbf{e} , and has a stationary point $\tilde{\mathbf{e}}$, corresponding to which

$$(11) \quad \mathbf{H}^{(k)\top} (\mathbf{H}^{(k)} \tilde{\mathbf{e}} - \mathbf{y}) + \delta \mathbf{W} \tilde{\mathbf{e}} = \mathbf{0},$$

where \mathbf{W} is a diagonal matrix with i^{th} diagonal entry given by $p(\tilde{e}_i^2 + \epsilon)^{p/2-1}$. Equation (11) is nonlinear in $\tilde{\mathbf{e}}$ since \mathbf{W} depends on $\tilde{\mathbf{e}}$, which makes a closed-form solution infeasible. Hence, we estimate the stationary point via the fixed-point iteration:

$$(12) \quad \mathbf{H}^{(k)\top} (\mathbf{H}^{(k)} \tilde{\mathbf{e}}^{(j+1, k)} - \mathbf{y}) + \delta \mathbf{W}^{(j, k)} \tilde{\mathbf{e}}^{(j+1, k)} = \mathbf{0},$$

where (j, k) indicates the j^{th} iterate corresponding to the fixed-point procedure within the k^{th} iteration of the Alt. Min. scheme, and $\mathbf{W}^{(j, k)}$ is a diagonal matrix whose i^{th} entry is $p((\tilde{e}_i^{(j, k)})^2 + \epsilon)^{p/2-1}$. The estimate $\tilde{\mathbf{e}}^{(j+1, k)}$ is computed according to the IRLS algorithm as

$$(13) \quad \tilde{\mathbf{e}}^{(j+1, k)} = \left(\mathbf{H}^{(k)\top} \mathbf{H}^{(k)} + \delta \mathbf{W}^{(j, k)} \right)^{-1} (\mathbf{H}^{(k)\top}) \mathbf{y}.$$

$\mathbf{W}^{(j, k)}$ tends to blow up for small values of $\tilde{e}_i^{(j, k)}$, which may happen as iterations progress, and might lead to ill-conditioning, causing problems in inversion. However, applying the matrix inversion lemma [23] circumvents the issue, for it gives,

$$(14) \quad \tilde{\mathbf{e}}^{(j+1, k)} = \mathbf{W}^{(j, k)^{-1}} (\mathbf{I} - \mathbf{H}^{(k)}) \left(\mathbf{I} + \mathbf{H}^{(k)} \delta \mathbf{W}^{(j, k)^{-1}} \mathbf{H}^{(k)\top} \right)^{-1} \mathbf{H}^{(k)} \mathbf{W}^{(j, k)^{-1}} \mathbf{H}^{(k)\top} \mathbf{y},$$

Algorithm 1 Alternating ℓ_p - ℓ_2 projections algorithm (ALPA) for sparse blind deconvolution.

Input: Measurement vector \mathbf{y}

Initialization: $k = 0$, $\mathbf{h}^{(0)} \in \mathbb{R}^L$, $\mathbf{H}^{(0)} = \text{Conv. Matrix}(\mathbf{h}^{(0)})$, $\mathbf{W}^{(0,0)} = \mathbf{I}_{M \times M}$, $\delta = 1$, set flag to FALSE.

While flag FALSE **do**

Step 1: *e-step*:

For $j = 1$ to J

$$\tilde{\mathbf{e}}^{(j+1,k)} = \mathbf{W}^{(j,k)^{-1}} (\mathbf{I} - \mathbf{H}^{(k)}) (\mathbf{I} + \mathbf{H}^{(k)} \delta \mathbf{W}^{(j,k)^{-1}} \mathbf{H}^{(k)\top})^{-1} \mathbf{H}^{(k)} \mathbf{W}^{(j,k)^{-1}} \mathbf{H}^{(k)\top} \mathbf{y}$$

end

$$\mathbf{e}^{(k+1)} = \tilde{\mathbf{e}}^{(J,k)}.$$

Step 2: Construct $\mathbf{E}^{(k+1)} = \text{Conv. Matrix}(\mathbf{e}^{(k+1)})$.

Step 3: *h-step*: $\mathbf{h}^{(k+1)} = \mathbf{E}^{(k+1)\dagger} \mathbf{y}$.

Step 4: Normalization: $\mathbf{h}^{(k+1)} \leftarrow \mathbf{h}^{(k+1)} / \|\mathbf{h}^{(k+1)}\|_2$.

Step 5: Update $\mathbf{H}^{(k+1)} = \text{Conv. Matrix}(\mathbf{h}^{(k+1)})$.

Step 6: Update $\mathbf{W}_{ii}^{(1,k+1)} = p \left((e_i^{(k+1)})^2 + \epsilon \right)^{p/2-1}$, $1 \leq i \leq N$.

Step 7: Stopping criterion: If $\frac{\|\mathbf{e}^{(k+1)} - \mathbf{e}^{(k)}\|_2^2}{\|\mathbf{e}^{(k)}\|_2^2} \leq \text{tolerance}$, then set flag to TRUE, $\mathbf{e}_{\text{opt}} = \mathbf{e}^{(k+1)}$, $\mathbf{h}_{\text{opt}} = \mathbf{h}^{(k+1)}$, else $k \leftarrow k + 1$.

end while

Outputs: \mathbf{e}_{opt} and \mathbf{h}_{opt} .

where $\mathbf{W}^{(j,k)^{-1}}$ is a diagonal matrix with i^{th} entry $p \left((\tilde{e}_i^{(j,k)})^2 + \epsilon \right)^{1-p/2}$. After J iterations of IRLS, we obtain the $(k+1)^{\text{st}}$ iterate for \mathbf{e} as $\mathbf{e}^{(k+1)} = \tilde{\mathbf{e}}^{(J,k)}$, which is then used to update $\mathbf{h}^{(k+1)}$ in the *h-step* as follows:

$$(15) \quad \mathbf{h}^{(k+1)} = \arg \min_{\mathbf{h}} F_{\epsilon}(\mathbf{h}, \mathbf{e}^{(k+1)}) = \arg \min_{\mathbf{h}} \|\mathbf{y} - \mathbf{E}^{(k+1)} \mathbf{h}\|_2^2 = \mathbf{E}^{(k+1)\dagger} \mathbf{y},$$

where $\mathbf{E}^{(k+1)} \in \mathbb{R}^{N \times L}$ is a linear convolution matrix constructed from $\mathbf{e}^{(k+1)}$, and \dagger denotes the Moore-Penrose inverse.

There is an inherent scale-ambiguity in the problem: if $\hat{\mathbf{h}}$ and $\hat{\mathbf{e}}$ constitute a solution pair, so do the scaled versions $\alpha \hat{\mathbf{h}}$ and $\hat{\mathbf{e}}/\alpha$, $\alpha \neq 0$. In order to overcome this ambiguity, we normalize the estimate of \mathbf{h} in every iteration, to possess unit energy, as follows: $\mathbf{h}^{(k)} \leftarrow \mathbf{h}^{(k)} / \|\mathbf{h}^{(k)}\|_2$. Alternatively, one could add the regularizer $\beta (\|\mathbf{h}\|^2 - 1)$, $\beta > 0$ to the cost F_{ϵ} in (15), which results in the update $\mathbf{h}^{(k+1)} = (\mathbf{E}^{(k+1)\top} \mathbf{E}^{(k+1)} + \beta \mathbf{I})^{-1} \mathbf{E}^{(k+1)\top} \mathbf{y}$.

The Alt. Min. scheme is summarized in Algorithm 1.

4. Error Reduction Properties. We next establish that, after every update of $\mathbf{h}^{(k)}$ and $\mathbf{e}^{(k)}$, the cost $F(\mathbf{h}^{(k)}, \mathbf{e}^{(k)})$ is upper-bounded by a non-increasing cost $F_{\epsilon}(\mathbf{h}^{(k)}, \mathbf{e}^{(k)})$, $\epsilon > 0$. We first consider the behavior of the cost functions F and F_{ϵ} for a fixed $\mathbf{h}^{(k)}$, but with the excitation estimated (Lemma 4.1), then with a fixed $\mathbf{e}^{(k)}$ and the filter estimated (Lemma 4.2). Finally, we combine the two results to get Lemma 4.3.

LEMMA 4.1. Let $\mathbf{e}^{(k+1)}$ be the minimizer of $F_\epsilon(\mathbf{h}^{(k)}, \mathbf{e})$ defined in (10) after the $(k+1)^{\text{st}}$ iteration, for a fixed $\mathbf{h}^{(k)}$. Then, F_ϵ satisfies the descent property

$$F_\epsilon(\mathbf{h}^{(k)}, \mathbf{e}^{(k+1)}) \leq F_\epsilon(\mathbf{h}^{(k)}, \mathbf{e}^{(k)}).$$

The proof is given in Appendix C.

LEMMA 4.2. Let $\mathbf{h}^{(k+1)}$ be the minimizer of $F_\epsilon(\mathbf{h}, \mathbf{e}^{(k+1)})$ defined in (15) after the $(k+1)^{\text{th}}$ iteration, for a given $\mathbf{e}^{(k+1)}$. Then, F_ϵ satisfies the descent property

$$F_\epsilon(\mathbf{h}^{(k+1)}, \mathbf{e}^{(k+1)}) \leq F_\epsilon(\mathbf{h}^{(k)}, \mathbf{e}^{(k+1)}).$$

Proof. From the analysis given in Section 2, we know that $\mathbf{E}^{(k+1)}$ consists of linearly independent columns. The Hessian of the cost function $F_\epsilon(\mathbf{h}, \mathbf{e}^{(k+1)}) = \|\mathbf{y} - \mathbf{E}^{(k+1)}\mathbf{h}\|_2^2$ is $\mathbf{E}^{(k+1)\text{T}}\mathbf{E}^{(k+1)}$, which is a positive-definite matrix. Consequently, $F_\epsilon(\mathbf{h}, \mathbf{e}^{(k+1)})$ is strictly convex, and hence $F_\epsilon(\mathbf{h}, \mathbf{e}^{(k+1)})$ has a unique minimizer, which we denote as $\mathbf{h}^{(k+1)}$. Thus, $F_\epsilon(\mathbf{h}^{(k+1)}, \mathbf{e}^{(k+1)}) \leq F_\epsilon(\mathbf{h}^{(k)}, \mathbf{e}^{(k+1)})$. ■

We haven't considered normalization of the filter estimate in the above proof. However, one could establish a similar property where the normalization is enforced via the regularizer $\beta(\|\mathbf{h}\|^2 - 1)$ alluded to at the end of Section 3.

Combining Lemmas 4.1 and 4.2 gives the following result pertaining to the descent of the cost F_ϵ after updating both filter and excitation.

LEMMA 4.3. Suppose $\mathbf{e}^{(k+1)}$ and $\mathbf{h}^{(k+1)}$ are the minimizers in (10) and (15), respectively. After the $(k+1)^{\text{st}}$ iteration of ALPA,

$$F_\epsilon(\mathbf{h}^{(k+1)}, \mathbf{e}^{(k+1)}) \leq F_\epsilon(\mathbf{h}^{(k)}, \mathbf{e}^{(k)}).$$

The following proposition establishes that, in every iteration, the difference between F_ϵ and F is bounded by a function of ϵ , which can be made arbitrarily small.

PROPOSITION 4.1. In every iteration of ALPA, the surrogate cost F_ϵ and the actual cost F satisfy the inequality:

$$0 < F_\epsilon(\mathbf{h}^{(k)}, \mathbf{e}^{(k)}) - F(\mathbf{h}^{(k)}, \mathbf{e}^{(k)}) \leq M\epsilon^{p/2}.$$

Proof. Consider the difference between the surrogate cost F_ϵ and the actual cost F :

$$(16) \quad F_\epsilon(\mathbf{h}^{(k)}, \mathbf{e}^{(k)}) - F(\mathbf{h}^{(k)}, \mathbf{e}^{(k)}) = \sum_{j=0}^{M-1} \underbrace{\left(\left(e_j^{(k)} \right)^2 + \epsilon \right)^{p/2} - \left(\left(e_j^{(k)} \right)^2 \right)^{p/2}}_{g_j^{(k)}(\epsilon)}.$$

The function $g_j^{(k)}(\epsilon)$ is symmetric in $e_j^{(k)}$ and has a maximum value of $\epsilon^{p/2}$ at $e_j^{(k)} = 0$, and a minimum value of 0 as $|e_j^{(k)}| \rightarrow \infty$. Therefore, $0 \leq g_j^{(k)}(\epsilon) \leq \epsilon^{p/2}$, which leads to the inequality $0 < F_\epsilon(\mathbf{h}^{(k)}, \mathbf{e}^{(k)}) - F(\mathbf{h}^{(k)}, \mathbf{e}^{(k)}) \leq M\epsilon^{p/2}$. ■

For illustration, consider a synthetic signal $y(n)$, which is the output of a filter excited by the sparse sequence of length 200 samples with Kronecker impulses at some randomly selected indices [10, 62, 85, 100, 150, 182]. The impulse response of the filter is chosen to be a sum of exponentially decaying sinusoids:

$$h(n) = \sum_{k=1}^3 e^{-\alpha_k n} \cos(\omega_k n) u(n), \quad n = 1, 2, \dots, 100; [\alpha_1, \alpha_2, \alpha_3] = [0.01, 0.014, 0.025],$$

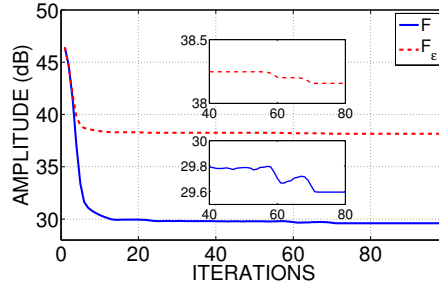


FIG. 1. (Color online) The cost functions F and F_ϵ (with $\epsilon = 10^{-6}$) pertaining to the example considered in Section 4.

and $[\omega_1, \omega_2, \omega_3] = [0.075, 0.138, 0.375]$. The observed signal $y(n)$ was deconvolved using ALPA with parameters chosen as $\lambda = 1$, $p = 0.1$, and $\epsilon = 10^{-6}$. The plots of the resulting cost functions F and F_ϵ are shown in Figure 1. Observe that the surrogate cost F_ϵ is non-increasing and upper-bounds F , which is not monotonic in general — this is an experimental confirmation of the result established in Lemma 4.3. The local variations in F are bounded as indicated by the following proposition.

PROPOSITION 4.2. *The ALPA, which minimizes $F_\epsilon(\mathbf{h}, \mathbf{e})$, leads to a sequence $F(\mathbf{h}^{(k)}, \mathbf{e}^{(k)})$ such that*

$$F(\mathbf{h}^{(k+1)}, \mathbf{e}^{(k+1)}) - F(\mathbf{h}^{(k)}, \mathbf{e}^{(k)}) \leq M\epsilon^{p/2}.$$

Proof. Using Lemma 4.3 and (16), we get that

$$F(\mathbf{h}^{(k+1)}, \mathbf{e}^{(k+1)}) < F(\mathbf{h}^{(k)}, \mathbf{e}^{(k)}) + \underbrace{\sum_{j=0}^{M-1} (g_j^{(k)}(\epsilon) - g_j^{(k+1)}(\epsilon))}_{\psi_{k+1}(\epsilon)}.$$

The function $\psi_{k+1}(\epsilon)$ is continuous in ϵ and $\lim_{\epsilon \rightarrow 0^+} \psi_{k+1}(\epsilon) = 0$. Also, from the proof of Proposition 4.1, both $g_j^{(k)}(\epsilon)$ and $g_j^{(k+1)}(\epsilon)$ are bounded as $0 \leq g_j^{(k)}(\epsilon), g_j^{(k+1)}(\epsilon) \leq \epsilon^{p/2}$. Hence, $\psi_{k+1} \leq |\psi_{k+1}| \leq M\epsilon^{p/2}$, which establishes the result. ■

5. Regularized Least-Squares Initialization and Concentration of Error. Since the cost $F_\epsilon(\mathbf{h}^{(k)}, \mathbf{e})$ in the e -step has local minima, initialization becomes important. In the blind case, the algorithm is initialized with a filter that we denote by $\tilde{\mathbf{h}}$. The weight matrix is initialized to $\mathbf{W}^{(0,0)} = \mathbf{I}_{M \times M}$, which results in the regularized LS estimate for the excitation. The error between the estimate and the true excitation depends on measurement noise. In the following analysis, we quantify the *concentration* of the estimate about the true value. The mean-absolute error (MAE) between $\mathbf{x} \in \mathbb{R}^M$ and its estimate $\hat{\mathbf{x}}$ is defined as

$$(17) \quad \text{MAE} = \frac{1}{M} \|\mathbf{x} - \hat{\mathbf{x}}\|_1.$$

Consider $\tilde{\mathbf{h}}$, an estimate of \mathbf{h}^* , which has the error $\Delta \mathbf{h} = \mathbf{h}^* - \tilde{\mathbf{h}}$. The convolution matrix constructed from $\tilde{\mathbf{h}}$ is given by $\tilde{\mathbf{H}} = \mathbf{H}^* + \Delta \mathbf{H}$, where $\Delta \mathbf{H}$ is the (error) convolution matrix corresponding to $\Delta \mathbf{h}$ and hence the Frobenius norm of $\Delta \mathbf{H}$ is related as $\|\Delta \mathbf{H}\|_F = \sqrt{M} \|\Delta \mathbf{h}\|_2$. Let $\|\Delta \mathbf{H}\|_2$ and $\|\mathbf{H}^*\|_2$ denote the matrix 2-norms

– these equal the largest singular values of the corresponding matrices. Using the matrix-norm equivalence $\|\Delta\mathbf{H}\|_2 \leq \|\Delta\mathbf{H}\|_F$, we have $\|\Delta\mathbf{H}\|_2 \leq \sqrt{M}\|\Delta\mathbf{h}\|_2$. We define *quasi-condition-number*¹ as $\kappa_q(\mathbf{H}) = \sigma_{\max}(\mathbf{H}) / (\sigma_{\min}^2(\mathbf{H}) + \delta)$. If we initialize $\mathbf{W}^{(0,0)} = \mathbf{I}_{M \times M}$, then we get the reg. LS solution $\hat{\mathbf{e}}_{\text{BRLS}} = (\tilde{\mathbf{H}}^T \tilde{\mathbf{H}} + \delta \mathbf{I})^{-1} \tilde{\mathbf{H}}^T \mathbf{y}$, which satisfies the equation: $(\tilde{\mathbf{H}}^T \tilde{\mathbf{H}} + \delta \mathbf{I}) \hat{\mathbf{e}}_{\text{BRLS}} = \tilde{\mathbf{H}}^T \mathbf{y}$. In terms of the ground-truth quantities \mathbf{H}^* and \mathbf{e}^* , we can write

$$(18) \quad ((\mathbf{H}^* + \Delta\mathbf{H})^T (\mathbf{H}^* + \Delta\mathbf{H}) + \delta \mathbf{I}) (\mathbf{e}^* + \Delta\mathbf{e}_{\text{BRLS}}) = (\mathbf{H}^* + \Delta\mathbf{H})^T (\mathbf{H}^* \mathbf{e}^* + \mathbf{w}),$$

where $\Delta\mathbf{e}_{\text{BRLS}} = \mathbf{e}^* - \hat{\mathbf{e}}_{\text{BRLS}}$ is the estimation error. An upper bound on MAE can be derived from (18) by rearranging the terms and employing properties of norms such as the triangle inequality and compatibility of norms. A detailed calculation is presented in Appendix D. The final expression for the bound turns out to be

$$(19) \quad \frac{1}{M} \|\Delta\mathbf{e}_{\text{BRLS}}\|_1 \leq \frac{1}{\sqrt{M}(1-2C_{\Delta\mathbf{h}})} \left((\kappa_q(\mathbf{H}^*) + C_{\Delta\mathbf{h}}) \|\mathbf{w}\|_2 + (\delta + C_{\Delta\mathbf{h}}) \|\mathbf{e}^*\|_2 \right).$$

The MAE between $\hat{\mathbf{e}}_{\text{BRLS}}$ and \mathbf{e}^* is concentrated as follows.

PROPOSITION 5.1. *Let $\tilde{\mathbf{h}}$ be an estimate of \mathbf{h}^* such that $\|\tilde{\mathbf{h}} - \mathbf{h}^*\|_2 = \|\Delta\mathbf{h}\|_2 < 1/(2\sqrt{M}\kappa_q(\mathbf{H}^*))$ and let the reg. LS estimate of \mathbf{e}^* be denoted as $\hat{\mathbf{e}}_{\text{BRLS}} = (\tilde{\mathbf{H}}^T \tilde{\mathbf{H}} + \delta \mathbf{I})^{-1} \tilde{\mathbf{H}}^T \mathbf{y}$. The MAE defined as $\frac{1}{M} \|\mathbf{e}^* - \hat{\mathbf{e}}_{\text{BRLS}}\|_1 = \frac{1}{M} \|\Delta\mathbf{e}_{\text{BRLS}}\|_1$ is upper bounded as in (19) and is concentrated as follows*

$$(20) \quad \mathcal{P} \left(\frac{1}{M} \|\Delta\mathbf{e}_{\text{BRLS}}\|_1 > \xi \right) \leq \frac{\sigma^2(\kappa_q(\mathbf{H}^*) + C_{\Delta\mathbf{h}})^2}{\left(\sqrt{M}(1-2C_{\Delta\mathbf{h}})\xi - (\delta + C_{\Delta\mathbf{h}}) \|\mathbf{e}^*\|_2 \right)^2},$$

where $C_{\Delta\mathbf{h}} = \sqrt{M}\kappa_q(\mathbf{H}^*)\|\Delta\mathbf{h}\|_2$.

The proof is given in Appendix E and is a consequence of the Markov inequality.

If the bound in (20) exceeds unity, it becomes trivial and noninformative. A nontrivial bound (i.e., a bound lesser than unity) is obtained when

$$(21) \quad \|\Delta\mathbf{h}\|_2 \leq \left(\frac{\xi / (\sigma\kappa_q(\mathbf{H}^*)) - 1}{(\sigma + 2)\sqrt{M} + \|\mathbf{e}^*\|_2} \right),$$

with $\xi \geq \sigma\kappa_q(\mathbf{H}^*)$.

The bound in (20) requires that the first- and second-order moments of noise be finite. In addition, if the noise is bounded, one can provide sharper bounds using the Hoeffding inequality stated below (recalled from Ch.2, pp. 34 of [6]).

THEOREM 5.1. (*Hoeffding's inequality*): *Suppose that X_1, X_2, \dots, X_M are M independent random variables with $\mathcal{E}\{X_i\} = \mu_i$ and $\mathcal{P}(X_i \in [a_i, b_i]) = 1$ with $a_i, b_i \in \mathbb{R}$, then*

$$\mathcal{P} \left(\frac{1}{M} \sum_{i=1}^M (X_i - \mu_i) > \xi \right) \leq \exp \left(- \frac{2M^2 \xi^2}{\sum_{i=1}^M (a_i - b_i)^2} \right), \quad \forall \xi > 0.$$

For the i.i.d. case, $X_i \in \mathcal{B}_{-a,a}$, $\mathcal{E}\{X_i\} = \mu$, the bound gets simplified to

$$(22) \quad \mathcal{P} \left(\frac{1}{M} \sum_{i=1}^M X_i - \mu > \xi \right) \leq \exp \left(- \frac{M\xi^2}{2a^2} \right), \quad \forall \xi > 0.$$

¹Note that the denominator in $\kappa_q(\mathbf{H})$ is the square of the smallest singular value.

Applying the Hoeffding inequality gives rise to the following result.

PROPOSITION 5.2. *Let \mathbf{w} be an i.i.d. random vector with $w_i \in \mathcal{B}_{-a,a}$, and $\mathcal{E}\{w_i^2\} = \sigma^2$. Then, for $\xi > 0$, the average error $\frac{1}{M}\|\Delta\mathbf{e}_{\text{BRLS}}\|_1$ is concentrated as*

$$(23) \quad \mathcal{P}\left(\frac{1}{M}\|\Delta\mathbf{e}_{\text{BRLS}}\|_1 > \xi\right) \leq \exp\left(\frac{-M}{2a^2}\left(\left(\frac{\sqrt{M}(1-2C_{\Delta\mathbf{h}})\xi - (\delta + C_{\Delta\mathbf{h}})\|\mathbf{e}^*\|_2}{\kappa_q(\mathbf{H}^*) + C_{\Delta\mathbf{h}}}\right)^2 - \sigma^2\right)^2\right).$$

Proof. Consider (37) and let

$$t = \frac{1}{M}\left(\frac{\sqrt{M}(1-2C_{\Delta\mathbf{h}})\xi - (\delta + C_{\Delta\mathbf{h}})\|\mathbf{e}^*\|_2}{\kappa_q(\mathbf{H}^*) + C_{\Delta\mathbf{h}}}\right)^2 - \mu.$$

Employing the Hoeffding bound gives

$$\mathcal{P}\left(\frac{1}{M}\|\mathbf{w}\|_2^2 - \mu > t\right) \leq \exp\left(\frac{Mt^2}{2a^2}\right),$$

from which (23) follows. \blacksquare

To gain some insights into the bound, consider the simpler case of non-blind deconvolution without regularization (i.e., $C_{\Delta\mathbf{h}} = 0, \delta = 0$), corresponding to which the error in excitation is denoted as $\Delta\mathbf{e}_{\text{LS}}$

$$(24) \quad \mathcal{P}\left(\frac{1}{M}\|\Delta\mathbf{e}_{\text{LS}}\|_1 > \xi\right) \leq \exp\left(-\frac{M^3}{2a^2}\left(\frac{\xi^2}{\kappa_q(\mathbf{H}^*)^2} - \frac{\sigma^2}{M}\right)^2\right).$$

For $\xi = n\sigma, n > 0$, we get

$$(25) \quad \mathcal{P}\left(\frac{1}{M}\|\Delta\mathbf{e}_{\text{LS}}\|_1 > n\sigma\right) \leq \exp\left(-\frac{M^3\sigma^4}{2a^2}\left(\frac{n^2}{\kappa_q(\mathbf{H}^*)^2} - \frac{1}{M}\right)^2\right).$$

For a random variable bounded over $[-a, a]$, the maximum variance is $\sigma^2 = a^2$ [6]. Taking this into account, the worst-case dependence on noise variance is expressed as

$$(26) \quad \mathcal{P}\left(\frac{1}{M}\|\Delta\mathbf{e}_{\text{LS}}\|_1 > na\right) \leq \exp\left(-\frac{M^3a^2}{2}\left(\frac{n^2}{\kappa_q(\mathbf{H}^*)^2} - \frac{1}{M}\right)^2\right).$$

6. Application to Speech Deconvolution. We next consider an application of the ALPA deconvolution technique to speech signals. Considering the LSI model for speech production [39, 45], a speech signal $y(n)$ can be expressed as a convolution of the vocal-tract impulse response $h(n)$ and excitation $e(n)$, as follows:

$$(27) \quad y(n) = (h * e)(n).$$

Depending on whether the speech segment is voiced or unvoiced, the excitation $e(n)$ is assumed to be a quasi-periodic impulse train or white noise, respectively [39]. In the case of voiced sounds, the impulses are placed at the instants of significant

excitation (referred to as *epochs* or glottal closure instants (GCIs)) [17, 41, 51], which depends on the pitch of the speaker. The vocal-tract configuration in producing a certain sound determines the frequency response of the filter. The vocal-tract impulse response is a convolution of exponentially decaying sinusoids, one corresponding to each resonance, and the excitation is sparse with one impulse per pitch cycle. The estimation of $h(n)$ and $e(n)$, given $y(n)$, is the problem of blind deconvolution and has widespread applications in speech analysis, coding, and recognition [45]. The *de facto* standard for speech deconvolution is based on linear prediction (LP), which relies on an autoregressive model for the vocal-tract filter, whose coefficients are estimated by minimizing the ℓ_2 -norm of the prediction error (also known as the *residue*) [39]. The residue has embedded in it information about epochs and pitch of the speaker [3, 41, 44].

Following the convolutional matrix notation established in Section 2, a vectorial representation of (27) is given by

$$(28) \quad \mathbf{y} = \mathbf{H}\mathbf{e} = \mathbf{E}\mathbf{h},$$

where $\mathbf{y} \in \mathbb{R}^N$, $\mathbf{h} \in \mathbb{R}^L$, and $\mathbf{e} \in \mathbb{R}^M$ are the speech, vocal-tract filter, and glottal excitation vectors, respectively. We employ ALPA to deconvolve the filter and the excitation (both of which are unknown) from the speech signal.

For experiments, we use speech utterances from the Western Michigan University database [24] (sampling frequency of 16 kHz). We excised a 30 ms long vowel segment corresponding to /æ/ from the utterance “had,” of a female speaker. ALPA was initialized with the LP filter and the excitation corresponding to model order 20. The parameters λ and p were set to 1 and 0.1, respectively, based on experimentation. The stopping criterion was typically met in about 20 iterations. The deconvolution results *vis-à-vis* LP estimates are shown in Figure 2. The excitation estimated by ALPA is sparse and quasi-periodic as opposed to the standard LP, which does not have a sparsity promoting regularizer. Even in the presence of AWGN (5 dB signal-to-noise ratio (SNR²), ALPA is robust (cf. Figure 3) and results in a sparse excitation (compare Figure 3(e) with Figure 2(e), in particular). The estimated filter was found to contain some noise, but lower than that present in the signal. The signal synthesized using the estimated excitation and the filter gave an SNR improvement of 4.5 dB, which shows that ALPA performs implicit denoising, which is an important feature of sparsity promoting formulations.

The excitation estimated by ALPA (cf. Figures 2(e) and 3(e)) is sparser than that estimated by LP (cf. Figures 2(b) and 3(b)). Although a sparse excitation model is used to motivate the LP formulation, the estimated excitation does not actually turn out to be sparse, primarily because the standard LP formulation does not explicitly incorporate any sparsity promoting constraints. This drawback was recently overcome by Giacobello et al. [21] who developed sparse LP. We shall next compare against this technique as well as the other sparse deconvolution techniques reported in the literature.

6.1. Comparisons With Sparse Deconvolution Methods. We next compare the performance of ALPA with a recently proposed smoothed one-over-two norm (SOOT) penalty-based blind deconvolution algorithm [47], and the *sparse linear prediction* (SLP) technique [21]. Further, we compare the sparse excitation estimated by ALPA with that obtained using the MM-based sparse deconvolution algorithm

²For the model $\mathbf{y} = \mathbf{x} + \mathbf{w}$, where \mathbf{x} denotes the signal (in \mathbb{R}^N) and $\mathbf{w} \sim \mathcal{N}(0, \sigma_w^2 \mathbf{I})$, the SNR is defined as $\text{SNR} = 10 \log_{10} \left(\frac{\|\mathbf{x}\|_2^2}{N\sigma_w^2} \right)$ dB.

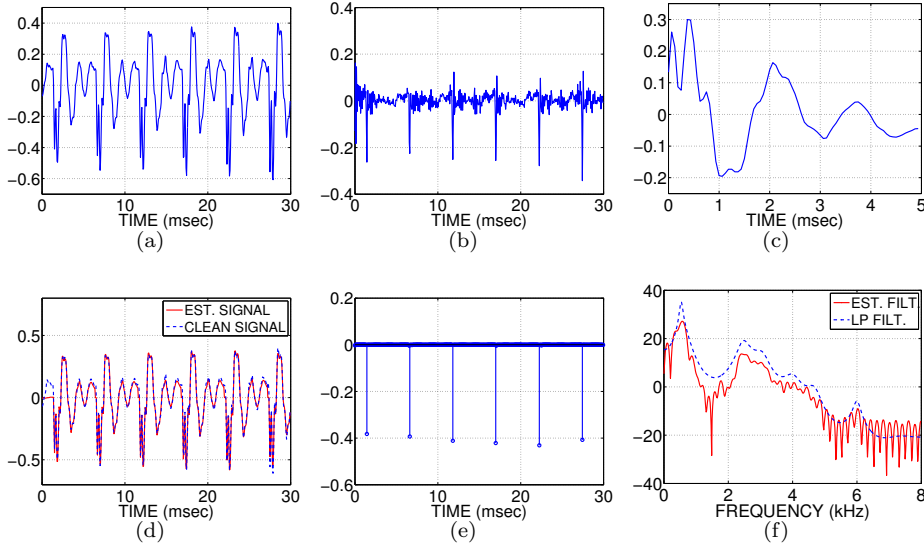


FIG. 2. (Color online) (a) A voiced segment /æ/ (female speaker) of length 480 samples (sampling rate 16 kHz); (b) LP residue (model order 20); (c) ALPA estimate of the filter; (d) comparison between the original vowel segment shown in (a) and that synthesized based on the estimated filter and excitation; (e) ALPA estimate of the excitation; and (f) frequency response of the estimated filter.

(SDMM) [48], which is a non-blind deconvolution algorithm. We briefly review the three techniques, before reporting performance comparisons.

6.1.1. The SOOT algorithm. The ℓ_1/ℓ_2 function, which is a ratio of the ℓ_1 and ℓ_2 norms, is scale-invariant and has been employed as a sparsity-promoting prior in the blind deconvolution of natural images [32]. However, since ℓ_1/ℓ_2 is non-convex and non-smooth, the blind deconvolution problem becomes difficult to solve. Repetti *et al.* [47] incorporated a smooth approximation of the ℓ_1/ℓ_2 function (smoothed one over two (SOOT)), which is the logarithm of the quotient of the smoothed ℓ_1 and ℓ_2 norms. An Alt. Min. approach combined with proximal methods is employed to optimize the cost function. In each step, Repetti *et al.* perform quadratic majorization of the smooth, non-convex cost function and minimize it using weighted proximal operators. The algorithm has been developed in the context of blind deconvolution of seismic signals and a MATLAB toolbox has been provided by the authors.

6.1.2. Sparse linear prediction (SLP). Giacobello *et al.* [21] introduced sparsity constraints within the LP framework. For a speech segment of length N , the model is represented in matrix form as $\mathbf{y} = \mathbf{Y}\mathbf{a} + \mathbf{r}$, where

$$\mathbf{y} = \begin{bmatrix} y(N_1) \\ \vdots \\ y(N_1 + N) \end{bmatrix}, \quad \mathbf{Y} = \begin{bmatrix} y(N_1 - 1) & \cdots & y(N_1 - P) \\ \vdots & \ddots & \vdots \\ y(N_1 + N - 1) & \cdots & y(N_1 + N - P) \end{bmatrix},$$

and P is the order of the predictor. They have proposed multiple formulations that yield either sparse residue or predictor coefficients or both. In particular, an ℓ_p -norm criterion is considered and the predictor coefficients corresponding to a

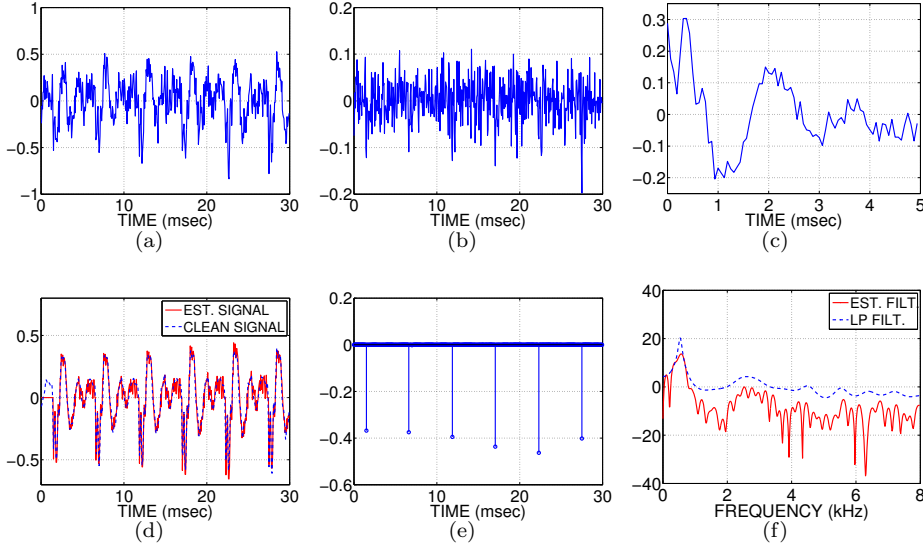


FIG. 3. (Color online) (a) A voiced segment /æ/ (female speaker) of length 480 samples (sampling rate 16 kHz, SNR = 5 dB); (b) LP residue (model order 20); (c) ALPA estimate of the filter; (d) comparison between the original clean vowel segment shown in Fig 2(a) and that synthesized based on the estimated filter and excitation. The improvement in SNR is 4.5 dB. (e) ALPA estimate of the excitation; and (f) frequency response of the estimated filter.

sparse residue are obtained as: $\mathbf{a}^* = \arg \min_{\mathbf{a}} \lim_{p \rightarrow 0} \|\mathbf{y} - \mathbf{Y}\mathbf{a}\|_p^p$. The cost is minimized using iteratively reweighted ℓ_1 minimization technique (IRL1) [10], where, in the k^{th} iteration, the predictor coefficient vector is $\mathbf{a}^{(k)} = \arg \min_{\mathbf{a}} \|\mathbf{W}^{(k-1)}(\mathbf{y} - \mathbf{Y}\mathbf{a})\|_1$, where $\mathbf{W}^{(k-1)} = \text{diag}(|\mathbf{y} - \mathbf{Y}\mathbf{a}^{(k-1)}| + 0.01)^{-1}$ (cf. Algorithm 1 in [21]). Typically, the IRL1 convergence criterion was met in five iterations.

6.1.3. MM-based sparse deconvolution (SDMM). In SDMM [48], one assumes that the speech signal \mathbf{y} is the output of an LP filter (finite-length approximation \mathbf{h}), excited by a sparse sequence \mathbf{e} . The excitation is obtained as a solution to the LASSO:

$$(29) \quad \mathbf{e}^* = \arg \min_{\mathbf{e}} \|\mathbf{y} - \mathbf{H}\mathbf{e}\|_2^2 + \delta \|\mathbf{e}\|_1,$$

computed using the IRLS approach, wherein the update utilizes the banded structure of the convolution matrix \mathbf{H} for efficient matrix inversion. Based on the optimality criterion satisfied by the minimizer of (29), a lower bound on the regularization parameter was derived in [48, 49] as $\delta \geq 3\sigma\|\mathbf{h}\|_2$, where σ is the noise variance.

6.1.4. Deconvolution results. We generated a synthetic vowel (/æ/, fundamental frequency $F_0 = 200$ Hz) speech segment (30 ms duration) using standard speech processing software accompanying [45]. We considered a 100-tap FIR filter, and prediction order 20 for SLP and SDMM. In the SOOT toolbox, Repetti *et al.* [47] consider a fixed set of noise standard deviations (0.01, 0.02, and 0.03) and optimized the regularization parameters accordingly. To ensure a fair comparison, we used the same noise conditions and parameter settings. The experiments were performed on an iMac with Intel® Core™ i5, 3.2 GHz, four-core processor.

TABLE 1

Comparison of MSE in the estimation of excitation, filter, and signal obtained using ALPA, SOOT, SLP, and SDMM.

Noise standard deviation \rightarrow		0.01	0.02	0.03
MSE in excitation (dB)	ALPA	-17.4	-10.7	-8.3
	SOOT	-2.0	-2.1	-2.2
	SLP	-0.04	0.46	0.74
	SDMM	-22.6	-11.0	-3.7
MSE in filter (dB)	ALPA	-15.0	-14.3	-10.0
	SOOT	-10.6	-10.0	-8.6
	SLP	-11.3	-7.5	-6.3
	SDMM	-10.9	-6.0	-4.1
MSE in reconstruction (dB)	ALPA	-21.6	-17.5	-14.1
	SOOT	-25.0	-19.6	-16.3
	SLP	-15.6	-12.0	-9.2
	SDMM	-12.5	-6.8	-4.6
Average time (sec.)	ALPA	0.1	0.1	0.2
	SOOT	1.3	1.3	1.3
	SLP	2.7	2.8	2.8
	SDMM	0.16	0.17	0.17

The MSE and MAE (defined in (17)) computed from the estimates of the excitation, filter, and the signal, averaged over 500 realizations of noise for the three noise variances considered are provided in Tables 1 and 2. To facilitate comparison, shifts in the estimated excitation and filter are compensated for by using the cyclic permutation operator. ALPA turned out to be consistently better than the other techniques in approximating the excitation and the filter. At higher SNR, SDMM is able to estimate the excitation with high accuracy, however, since no refinement is involved in the LP filter, it is unable to provide a good approximation to the ground-truth filter. A lower MAE in the estimation of the excitation in the case of both ALPA and SDMM indicates that the estimates are sparse and more accurate than SOOT. However, ALPA gives sharper peaks than SDMM. The SLP did not estimate the excitation accurately.

The results for a natural vowel segment /æ/ of 30 ms duration uttered by a female speaker under clean and noisy conditions (SNR = 10 dB) are shown in Figures 4 and 5. To remove variability due to scale across the techniques and facilitate fair comparison, the excitations shown in Row 3 of Figures 4 and 5 have been rescaled to possess unit energy.

We observe that ALPA, SOOT, and SDMM yield sparse excitations in both clean and noisy conditions, with ALPA resulting in the sparsest excitation. The spectral estimates of the vocal-tract filter are similar for ALPA and SOOT. In the case of SLP, we observe that the excitation is *peakier* than the LP residue, but not as sparse as what the other techniques give, and especially under noisy conditions, the uncorrelated noise appears in the residue.

7. Conclusions. We considered the problem of blind deconvolution of signals obtained as the output of a smooth filter excited with a sparse sequence. The sparseness of the excitation has been incorporated in the formulation by modeling it as a random vector with i.i.d. entries coming from a heavy-tailed gpG distribution. In the presence of AWGN, the cost function turned out to be non-convex and non-smooth, to optimize which we relied on an Alt. Min. scheme. The proposed algorithm ALPA optimizes a smooth, non-convex proxy for the original cost function by alternating between two

TABLE 2

Comparison of MAE in the estimation of excitation, filter, and signal obtained using ALPA, SOOT, SLP, and SDMM.

Noise standard deviation →		0.01	0.02	0.03
MAE in excitation (dB)	ALPA	-6.8	-4.0	-1.4
	SOOT	3.8	3.6	3.4
	SLP	10.6	11.0	11.2
	SDMM	-8.7	-2.3	1.7
MAE in filter (dB)	ALPA	0.9	1.1	3.6
	SOOT	2.6	3.1	3.8
	SLP	2.0	4.0	4.4
	SDMM	3.0	5.5	6.3
MAE in reconstruction (dB)	ALPA	-0.3	2.5	4.2
	SOOT	-1.2	1.6	3.3
	SLP	3.7	5.5	7.0
	SDMM	5.7	8.5	9.5

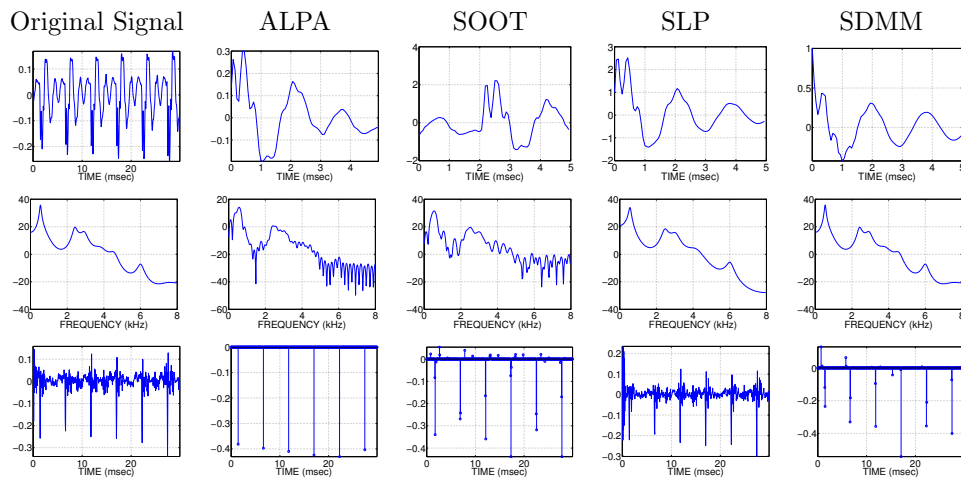


FIG. 4. (Color online) A comparison of sparse deconvolution methods for clean speech: Rows 1, 2, and 3 corresponding to Column 1 show the speech signal, frequency response of the LP filter, and the LP residue, respectively. For Columns 2–5, Rows 1, 2, and 3 show estimates of the filter, its frequency response, and the excitation, respectively.

steps, namely, the e -step for optimizing the excitation and the h -step for optimizing the filter. The individual steps consider a convex relaxation of the original cost function. We also proved that, with iterations, the reduction in the actual cost is upper-bounded by the reduction in the ϵ -regularized surrogate cost, which in turn is non-increasing. This error reduction property ensures that, in practice, the iterations converge to a reasonable solution, a behavior that was also verified experimentally. As far as initialization is concerned, we considered the suitability of the regularized pseudo-inverse solution and established probabilistic guarantees on its distance from the ground-truth, which depends on the noise level, the condition number of the system, error in initial estimate of the filter, and regularization parameter. For bounded noise, the probabilistic bounds were tightened using Hoeffding's inequality. We then demonstrated an application of ALPA for blind deconvolution of voiced speech signals, into the smooth vocal tract and sparse excitation components. A comparison of the

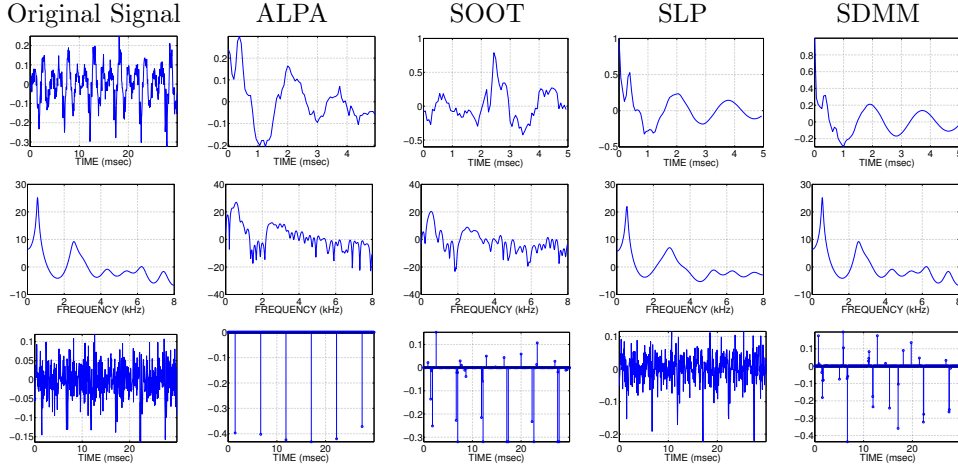


FIG. 5. (Color online) A comparison of sparse deconvolution methods for noisy speech (SNR = 10 dB): Rows 1, 2, and 3 corresponding to Column 1 show the speech signal, frequency response of the LP filter, and the LP residue, respectively. For Columns 2–5, Rows 1, 2, and 3 show estimates of the filter, its frequency response, and the excitation, respectively. Comparing the excitations, ALPA yields the sparsest excitation.

excitations obtained using ALPA, SOOT, SLP, and SDMM showed that ALPA yields the sparsest excitation and is also the fastest computationally.

Appendix A. Proof of Lemma 2.1. Consider the convolution matrix

$$(30) \quad \mathbf{H} = \begin{bmatrix} h(0) & 0 & \dots & 0 \\ h(1) & h(0) & \dots & 0 \\ h(2) & h(1) & \dots & 0 \\ \vdots & \vdots & \ddots & \vdots \\ h(L-1) & h(L-2) & \dots & \dots \\ 0 & h(L-1) & \dots & \dots \\ 0 & 0 & \dots & \dots \\ \vdots & \vdots & \ddots & \vdots \\ 0 & 0 & \dots & h(L-1) \end{bmatrix}.$$

We assume, without loss of generality, that $h(0) \neq 0$. The first entry of the vector $\sum_{s=0}^{M-1} \gamma_s \mathbf{h}_s$ will be zero if and only if $\gamma_0 = 0$. Similarly, the second entry will be zero if and only if $\gamma_0 = \gamma_1 = 0$. By mathematical induction, $\sum_{s=0}^{M-1} \gamma_s \mathbf{h}_s = \mathbf{0}$ if and only if $\gamma_s = 0, \forall s$. Hence, $\{\mathbf{h}_s\}_{s=0}^{M-1}$ are linearly independent. From the definition of Riesz bases in finite-dimensional vector spaces [40], the Riesz bounds are given by the infimum and supremum of the quotient $\frac{\|\mathbf{H}\mathbf{x}\|_2^2}{\|\mathbf{x}\|_2^2}, \forall \mathbf{x} \in \mathbb{R}^M - \{\mathbf{0}\}$, which is, in fact, the Rayleigh quotient, and hence (7) follows. ■

Appendix B. Proof of Proposition 2.1. Denote $\mathbf{R}_{\mathbf{h}\mathbf{h}} = \mathbf{H}^T \mathbf{H}$, with its entries (s_1, s_2) containing the autocorrelation terms corresponding to \mathbf{h} , that is,

$$(31) \quad [\mathbf{R}_{\mathbf{h}\mathbf{h}}]_{s_1, s_2} = \begin{cases} \mathbf{h}_{s_1}^T \mathbf{h}_{s_2} = \mathbf{h}_{s_2}^T \mathbf{h}_{s_1} & \text{for } s_1 \neq s_2, \\ 1 & \text{for } s_1 = s_2. \end{cases}$$

The entries also satisfy $\mathbf{R}_{\mathbf{h}\mathbf{h}}(s_1, s_2) = r_{\mathbf{h}\mathbf{h}}(|s_1 - s_2|)$. In order to find the range of values $\sigma_{\min}^2(\mathbf{H})$ can take, we use the Gerschgorin disc theorem [25]. Due to the unit-norm constraint on \mathbf{h} , all the Gerschgorin discs pertaining to $\mathbf{H}^T\mathbf{H}$ will be centered at $1 + 0i$. Since $\mathbf{H}^T\mathbf{H}$ is symmetric, all eigenvalues will be real. According to Gerschgorin disc

theorem, we have $\sigma_{\min}^2(\mathbf{H}) \geq 1 - \max_{s_1} \left(\sum_{s_2=0, s_2 \neq s_1}^{M-1} |[\mathbf{R}_{\mathbf{h}\mathbf{h}}]_{s_1, s_2}| \right)$. If M is odd, then

the $((M-1)/2)^{\text{th}}$ row of $\mathbf{R}_{\mathbf{h}\mathbf{h}}$ contains autocorrelation terms corresponding to all the lags to both left and right of $\mathbf{R}_{\mathbf{h}\mathbf{h}}(\frac{M-1}{2}, \frac{M-1}{2})$ and hence the absolute sum of the elements of the row excluding the diagonal element will be the largest. Thus,

$\sigma_{\min}^2(\mathbf{H}) \geq 1 - 2 \left(\sum_{\ell=1}^{(M-1)/2} |r_{\mathbf{h}\mathbf{h}}(\ell)| \right)$. In order to ensure that $0 < \eta \leq \sigma_{\min}^2(\mathbf{H}) \leq 1$,

we require that $0 \leq \sum_{\ell=1}^{(M-1)/2} |r_{\mathbf{h}\mathbf{h}}(\ell)| \leq \frac{1-\eta}{2}$. Similarly, σ_{\max}^2 will also be contained

within a circle of radius $\sigma_{\max}^2(\mathbf{H}) \leq 1 + 2 \sum_{\ell=1}^{(M-1)/2} |r_{\mathbf{h}\mathbf{h}}(\ell)|$. \blacksquare

Appendix C. Proof of Lemma 4.1. The difference

$$F_{\epsilon}(\mathbf{h}^{(k)}, \mathbf{e}^{(k)}) - F_{\epsilon}(\mathbf{h}^{(k)}, \mathbf{e}^{(k+1)}) = \delta \sum_{j=0}^{M-1} \left(\left((e_j^{(k)})^2 + \epsilon \right)^{p/2} - \left((e_j^{(k+1)})^2 + \epsilon \right)^{p/2} \right) + \left(\|\mathbf{y} - \mathbf{H}^{(k)}\mathbf{e}^{(k)}\|_2^2 - \|\mathbf{y} - \mathbf{H}^{(k)}\mathbf{e}^{(k+1)}\|_2^2 \right),$$

can be rearranged as

$$F_{\epsilon}(\mathbf{h}^{(k)}, \mathbf{e}^{(k)}) - F_{\epsilon}(\mathbf{h}^{(k)}, \mathbf{e}^{(k+1)}) = \delta \sum_{j=0}^{M-1} \left(\left((e_j^{(k)})^2 + \epsilon \right)^{p/2} - \left((e_j^{(k+1)})^2 + \epsilon \right)^{p/2} \right) + \left\| \mathbf{H}^{(k)}\mathbf{e}^{(k)} - \mathbf{H}^{(k)}\mathbf{e}^{(k+1)} \right\|^2 + \left(\mathbf{y} - \mathbf{H}^{(k)}\mathbf{e}^{(k+1)} \right)^T \left(\mathbf{H}^{(k)}\mathbf{e}^{(k+1)} - \mathbf{H}^{(k)}\mathbf{e}^{(k)} \right).$$

The last term is simplified by using (12) as,

$$F_{\epsilon}(\mathbf{h}^{(k)}, \mathbf{e}^{(k)}) - F_{\epsilon}(\mathbf{h}^{(k)}, \mathbf{e}^{(k+1)}) = \left\| \mathbf{H}^{(k)}\mathbf{e}^{(k)} - \mathbf{H}^{(k)}\mathbf{e}^{(k+1)} \right\|_2^2 + \delta \sum_{j=0}^{M-1} \underbrace{\left(\left((e_j^{(k)})^2 + \epsilon \right)^{p/2} - \left((e_j^{(k+1)})^2 + \epsilon \right)^{p/2} - p \frac{e_j^{(k+1)} (e_j^{(k)} - e_j^{(k+1)})}{\left((e_j^{(k)})^2 + \epsilon \right)^{(1-p/2)}} \right)}_{T_j}.$$

Consider the term T_j inside the summation:

$$\frac{\left((e_j^{(k)})^2 + \epsilon \right) - \left((e_j^{(k+1)})^2 + \epsilon \right)^{(p/2)} \left((e_j^{(k)})^2 + \epsilon \right)^{(1-p/2)}}{\left((e_j^{(k)})^2 + \epsilon \right)^{(1-p/2)}} - p e_j^{(k+1)} (e_j^{(k)} - e_j^{(k+1)})$$

Applying the inequality: arithmetic mean \geq geometric mean, to the term inside the box, we get

$$\left(\left(e_j^{(k+1)} \right)^2 + \epsilon \right)^{(p/2)} \left(\left(e_j^{(k)} \right)^2 + \epsilon \right)^{(1-p/2)} \leq \frac{p}{2} \left(\left(e_j^{(k+1)} \right)^2 + \epsilon \right) + \left(1 - \frac{p}{2} \right) \left(\left(e_j^{(k)} \right)^2 + \epsilon \right).$$

As a result,

$$\begin{aligned} T_j &\geq \frac{\left(\left(e_j^{(k)} \right)^2 + \epsilon \right) - \frac{p}{2} \left(\left(e_j^{(k+1)} \right)^2 + \epsilon \right) - \left(1 - \frac{p}{2} \right) \left(\left(e_j^{(k)} \right)^2 + \epsilon \right) - p e_j^{(k+1)} \left(e_j^{(k)} - e_j^{(k+1)} \right)}{\left(\left(e_j^{(k)} \right)^2 + \epsilon \right)^{(1-p/2)}} \\ &= \frac{p \left(e_j^{(k)} - e_j^{(k+1)} \right)^2}{\left(\left(e_j^{(k)} \right)^2 + \epsilon \right)^{(1-p/2)}} \geq 0. \end{aligned}$$

$$\begin{aligned} \text{Consequently, } F_\epsilon \left(\mathbf{h}^{(k)}, \mathbf{e}^{(k)} \right) - F_\epsilon \left(\mathbf{h}^{(k)}, \mathbf{e}^{(k+1)} \right) &\geq \left\| \mathbf{H}^{(k)} \left(\mathbf{e}^{(k)} - \mathbf{e}^{(k+1)} \right) \right\|_2^2 \geq 0, \\ &\Rightarrow F_\epsilon \left(\mathbf{h}^{(k)}, \mathbf{e}^{(k+1)} \right) \leq F_\epsilon \left(\mathbf{h}^{(k)}, \mathbf{e}^{(k)} \right). \end{aligned}$$

■

Appendix D. Upper Bound on MAE. Expanding (18) and rearranging terms, we get

$$(32) \quad \begin{aligned} \left(\mathbf{H}^{*\top} \mathbf{H}^* + \delta \mathbf{I} \right) \Delta \mathbf{e}_{\text{BRLS}} &= \left(\mathbf{H}^* + \Delta \mathbf{H} \right)^\top \mathbf{w} - \left(\mathbf{H}^{*\top} \Delta \mathbf{H} + \Delta \mathbf{H}^\top \Delta \mathbf{H} + \delta \right) \mathbf{e}^* \\ &\quad - \left(\mathbf{H}^{*\top} \Delta \mathbf{H} + \Delta \mathbf{H}^\top \mathbf{H}^* + \Delta \mathbf{H}^\top \Delta \mathbf{H} \right) \Delta \mathbf{e}_{\text{BRLS}}. \end{aligned}$$

Using the triangle inequality, $\|\mathbf{A} + \mathbf{B}\|_2 \leq \|\mathbf{A}\|_2 + \|\mathbf{B}\|_2$ and compatibility of induced norms, $\|\mathbf{A}\mathbf{x}\|_2 \leq \|\mathbf{A}\|_2 \|\mathbf{x}\|_2$ gives

$$\begin{aligned} \|\Delta \mathbf{e}_{\text{BRLS}}\|_2 &\leq \left\| \left(\mathbf{H}^{*\top} \mathbf{H}^* + \delta \mathbf{I} \right)^{-1} \right\|_2 \left\{ \|\mathbf{H}^* + \Delta \mathbf{H}\|_2 \|\mathbf{w}\|_2 + \right. \\ &\quad \left. \left(\|\mathbf{H}^*\|_2 \|\Delta \mathbf{H}\|_2 + \|\Delta \mathbf{H}\|_2^2 + \delta \right) \|\mathbf{e}^*\|_2 + \left(2\|\mathbf{H}^*\|_2 \|\Delta \mathbf{H}\|_2 + \|\Delta \mathbf{H}\|_2^2 \right) \|\Delta \mathbf{e}_{\text{BRLS}}\|_2 \right\}. \end{aligned}$$

Now, $\|\Delta \mathbf{H}\|_2 \leq \sqrt{M} \|\Delta \mathbf{h}\|_2$ and hence, $\|\mathbf{H}^* + \Delta \mathbf{H}\|_2 \leq \|\mathbf{H}^*\|_2 + \|\Delta \mathbf{H}\|_2 \leq \|\mathbf{H}^*\|_2 + \sqrt{M} \|\Delta \mathbf{h}\|_2$. Since $\left\| \left(\mathbf{H}^{*\top} \mathbf{H}^* + \delta \mathbf{I} \right)^{-1} \right\|_2 \|\mathbf{H}^*\|_2 = \kappa_q(\mathbf{H}^*)$ and $\|\mathbf{H}^*\|_2 \geq 1$, the term $\sqrt{M} \left\| \left(\mathbf{H}^{*\top} \mathbf{H}^* + \delta \mathbf{I} \right)^{-1} \right\|_2 \|\Delta \mathbf{h}\|_2 \|\mathbf{w}\|_2 \leq \sqrt{M} \left\| \left(\mathbf{H}^{*\top} \mathbf{H}^* + \delta \mathbf{I} \right)^{-1} \right\|_2 \|\mathbf{H}^*\|_2 \|\Delta \mathbf{h}\|_2 \|\mathbf{w}\|_2 = \sqrt{M} \kappa_q \|\mathbf{H}^*\|_2 \|\mathbf{w}\|_2$. Therefore,

$$(33) \quad \begin{aligned} \|\Delta \mathbf{e}_{\text{BRLS}}\|_2 &\leq \left(\kappa_q(\mathbf{H}^*) + \sqrt{M} \kappa_q(\mathbf{H}^*) \|\Delta \mathbf{h}\|_2 \right) \|\mathbf{w}\|_2 + \left(\sqrt{M} \kappa_q(\mathbf{H}^*) \|\Delta \mathbf{h}\|_2 + \delta \right) \|\mathbf{e}^*\|_2 \\ &\quad + 2\sqrt{M} \kappa_q(\mathbf{H}^*) \|\Delta \mathbf{h}\|_2 \|\Delta \mathbf{e}_{\text{BRLS}}\|_2 + \mathcal{O}(\|\Delta \mathbf{h}\|_2^2). \end{aligned}$$

Neglecting the $\mathcal{O}(\|\Delta \mathbf{h}\|_2^2)$ terms,

$$(34) \quad \begin{aligned} \left(1 - 2\sqrt{M} \kappa_q(\mathbf{H}^*) \|\Delta \mathbf{h}\|_2 \right) \|\Delta \mathbf{e}_{\text{BRLS}}\|_2 &\leq \\ \left(\kappa_q(\mathbf{H}^*) + \sqrt{M} \kappa_q(\mathbf{H}^*) \|\Delta \mathbf{h}\|_2 \right) \|\mathbf{w}\|_2 &+ \left(\sqrt{M} \kappa_q(\mathbf{H}^*) \|\Delta \mathbf{h}\|_2 + \delta \right) \|\mathbf{e}^*\|_2. \end{aligned}$$

Denoting $\sqrt{M}\kappa_q(\mathbf{H}^*)\|\Delta\mathbf{h}\|_2 = C_{\Delta\mathbf{h}}$. If $C_{\Delta\mathbf{h}} < \frac{1}{2}$, then

$$(35) \quad \|\Delta\mathbf{e}_{\text{BRLS}}\|_2 \leq \frac{1}{(1-2C_{\Delta\mathbf{h}})} \left\{ (\kappa_q(\mathbf{H}^*) + C_{\Delta\mathbf{h}}) \|\mathbf{w}\|_2 + (C_{\Delta\mathbf{h}} + \delta) \|\mathbf{e}^*\|_2 \right\}.$$

Using equivalence of norms $\frac{1}{\sqrt{M}}\|\Delta\mathbf{e}_{\text{BRLS}}\|_1 \leq \|\Delta\mathbf{e}_{\text{BRLS}}\|_2$, we get (19). \blacksquare

Appendix E. Proof of Proposition 5.1. In view of the inequality in (19),

$$(36) \quad \mathcal{P} \left(\frac{1}{M} \|\Delta\mathbf{e}_{\text{BRLS}}\|_1 > \xi \right) < \mathcal{P} \left(\frac{1}{\sqrt{M}(1-2C_{\Delta\mathbf{h}})} \left\{ (\kappa_q(\mathbf{H}^*) + C_{\Delta\mathbf{h}}) \|\mathbf{w}\|_2 + (\delta + C_{\Delta\mathbf{h}}) \|\mathbf{e}^*\|_2 \right\} > \xi \right).$$

Rearranging the right-hand side terms and using Markov inequality, we get

$$(37) \quad \mathcal{P} \left(\|\mathbf{w}\|_2^2 > \left(\frac{\sqrt{M}(1-2C_{\Delta\mathbf{h}})\xi - (\delta + C_{\Delta\mathbf{h}}) \|\mathbf{e}^*\|_2}{\kappa_q(\mathbf{H}^*) + C_{\Delta\mathbf{h}}} \right)^2 \right) < \frac{\mathcal{E}(\|\mathbf{w}\|_2^2)(\kappa_q(\mathbf{H}^*) + C_{\Delta\mathbf{h}})^2}{\left(\sqrt{M}(1-2C_{\Delta\mathbf{h}})\xi - (\delta + C_{\Delta\mathbf{h}}) \|\mathbf{e}^*\|_2 \right)^2}.$$

Since the entries of \mathbf{w} are i.i.d., $\mathcal{E}(\|\mathbf{w}\|_2^2) = M\sigma^2$, which results in the inequality (20). \blacksquare

Acknowledgments. The authors would like to thank Subhadip Mukherjee and Bastya Ajay Shenoy for fruitful technical discussions.

REFERENCES

- [1] A. AHMED, B. RECHT, AND J. ROMBERG, *Blind deconvolution using convex programming*, IEEE Trans. Inf. Theory, 60 (2014), pp. 1711–1732.
- [2] M. ALMEIDA AND M. FIGUEIREDO, *Deconvolving images with unknown boundaries using the alternating direction method of multipliers*, IEEE Trans. Image Process., 22 (2013), pp. 3084–3096.
- [3] T. V. ANANTHAPADMANABHA AND B. YEGNANARAYANA, *Epoch extraction from linear prediction residual for identification of closed glottis interval*, IEEE Trans. Acoust., Speech, Signal Process., 27 (1979), pp. 309–319.
- [4] A. BECK AND M. TEBoulLE, *A fast iterative shrinkage-thresholding algorithm for linear inverse problems*, SIAM J. Imag. Sci., 2 (2009), pp. 183–202.
- [5] A. BENICHOX, E. VINCENT, AND R. GRIBONVAL, *A fundamental pitfall in blind deconvolution with sparse and shift-invariant priors*, in Proc. IEEE Int. Conf. Acoust., Speech, Signal Process., May 2013, pp. 6108–6112.
- [6] S. BOUCHERON, G. LUGOSI, AND P. MASSART, *Concentration Inequalities: A Nonasymptotic Theory of Independence*, Oxford University Press, 2013.
- [7] M. M. BRONSTEIN, A. M. BRONSTEIN, M. ZIBULEVSKY, AND Y. Y. ZEEVI, *Blind deconvolution of images using optimal sparse representations*, IEEE Trans. Image Process., 14 (2005), pp. 726–736.
- [8] P. CAMPISI AND K. EGIAZARIAN, *Blind Image Deconvolution: Theory and Applications*, CRC press, 2007.
- [9] E. J. CANDÈS, J. K. ROMBERG, AND T. TAO, *Stable signal recovery from incomplete and inaccurate measurements*, Commun. Pure Appl. Math., 59 (2006), pp. 1207–1223.
- [10] E. J. CANDÈS, M. B. WAKIN, AND S. P. BOYD, *Enhancing sparsity by reweighted ℓ_1 minimization*, J. Fourier Anal. Applicat., 14 (2008), pp. 877–905.

- [11] R. CHARTRAND, *Exact reconstruction of sparse signals via nonconvex minimization*, IEEE Signal Process. Lett., 14 (2007), pp. 707–710.
- [12] R. CHARTRAND AND W. YIN, *Iteratively reweighted algorithms for compressive sensing*, in Proc. IEEE Int. Conf. Acoust., Speech, Signal Process., Mar. 2008, pp. 3869–3872.
- [13] S. S. CHEN, D. L. DONOHO, AND M. A. SAUNDERS, *Atomic decomposition by basis pursuit*, SIAM J. Sci. Comp., 20 (1998), pp. 33–61.
- [14] Y. CHI, *Guaranteed blind sparse spikes deconvolution via lifting and convex optimization*, IEEE J. Selected Topics Signal Process., 10 (2016), pp. 782–794.
- [15] S. CHOUDHARY AND U. MITRA, *Sparse blind deconvolution: What cannot be done*, in Proc. IEEE Int. Symp. Inf. Theory, June 2014, pp. 3002–3006.
- [16] I. DAUBECHIES, R. DEVORE, M. FORNASIER, AND C. S. GÜNTÜRK, *Iteratively reweighted least squares minimization for sparse recovery*, Commun. Pure Appl. Math., 63 (2010), pp. 1–38.
- [17] T. DRUGMAN, M. THOMAS, J. GUDNASON, P. NAYLOR, AND T. DUTOIT, *Detection of glottal closure instants from speech signals: A quantitative review*, IEEE Trans. Audio, Speech, Language Process., 20 (2012), pp. 994–1006.
- [18] R. FERGUS, B. SINGH, A. HERTZMANN, S. T. ROWEIS, AND W. T. FREEMAN, *Removing camera shake from a single photograph*, 25 (2006), pp. 787–794.
- [19] M. FIGUEIREDO AND R. D. NOWAK, *An EM algorithm for wavelet-based image restoration*, IEEE Trans. Image Process., 12 (2003), pp. 906–916.
- [20] M. FIGUEIREDO, R. D. NOWAK, AND S. J. WRIGHT, *Gradient projection for sparse reconstruction: Application to compressed sensing and other inverse problems*, IEEE J. Sel. Topics Signal Process., 1 (2007), pp. 586–597.
- [21] D. GIACOBELLO, M. CHRISTENSEN, M. MURTHI, S. JENSEN, AND M. MOONEN, *Sparse linear prediction and its applications to speech processing*, IEEE Trans. Audio, Speech, Language Process., 20 (2012), pp. 1644–1657.
- [22] G. H. GOLUB, M. HEATH, AND G. WAHBA, *Generalized cross-validation as a method for choosing a good ridge parameter*, Technometrics, 21 (1979), pp. 215–223.
- [23] G. H. GOLUB AND C. F. VAN LOAN, *Matrix Computations*, Johns Hopkins University Press, Baltimore, MD, USA, 3 ed., 1996.
- [24] J. M. HILLENBRAND, *Vowel database*. <http://homepages.wmich.edu/~hillenbr/voweldata.html>.
- [25] R. A. HORN AND C. R. JOHNSON, *Matrix Analysis*, Cambridge University Press, 2012.
- [26] D. R. HUNTER AND K. LANGE, *Quantile regression via an MM algorithm*, J. Comput. Graphical Stat., 9 (2000), pp. 60–77.
- [27] B. D. JEFFS AND M. GUNSAY, *Restoration of blurred star field images by maximally sparse optimization*, IEEE Trans. Image Process., 2 (1993), pp. 202–211.
- [28] N. JOSHI, C. L. ZITNICK, R. SZELISKI, AND D. J. KRIEGMAN, *Image deblurring and denoising using color priors*, in IEEE Conf. Computer Vision Pattern Recognition, June 2009, pp. 1550–1557.
- [29] A. KATSAGGELOS AND K. LAY, *Maximum likelihood blur identification and image restoration using the EM algorithm*, IEEE Trans. Signal Process., 39 (1991), pp. 729–733.
- [30] J. KOTERA, F. ŠROUBEK, AND P. MILANFAR, *Blind deconvolution using alternating maximum a posteriori estimation with heavy-tailed priors*, in Comput. Anal. Images Patterns, Springer, 2013, pp. 59–66.
- [31] D. KRISHNAN AND R. FERGUS, *Fast image deconvolution using hyper-Laplacian priors*, in Advances Neural Information Processing Systems, 2009, pp. 1033–1041.
- [32] D. KRISHNAN, T. TAY, AND R. FERGUS, *Blind deconvolution using a normalized sparsity measure*, in Proc. IEEE Intl. Conf. Comput. Vision, Pattern Recognition, Jun. 2011, pp. 233–240.
- [33] D. KUNDUR AND D. HATZINAKOS, *Blind image deconvolution*, IEEE Signal Process. Mag., 13 (1996), pp. 43–64.
- [34] M.-J. LAI AND J. WANG, *An unconstrained ℓ_q minimization with $0 < q \leq 1$ for sparse solution of underdetermined linear systems*, SIAM J. Optimization, 21 (2011), pp. 82–101.
- [35] A. LEVIN, R. FERGUS, F. DURAND, AND W. T. FREEMAN, *Image and depth from a conventional camera with a coded aperture*, ACM Trans. Graphics, 26 (2007), p. 70.
- [36] A. LEVIN, Y. WEISS, F. DURAND, AND W. FREEMAN, *Understanding blind deconvolution algorithms*, IEEE Trans. Pattern Anal. Mach. Intell., 33 (2011), pp. 2354–2367.
- [37] Y. LI, K. LEE, AND Y. BRESLER, *Identifiability in blind deconvolution with subspace or sparsity constraints*, IEEE Trans. Inf. Theory, PP (2016), pp. 1–1.
- [38] C. LIKAS AND N. GALATSANOS, *A variational approach for Bayesian blind image deconvolution*, IEEE Trans. Signal Process., 52 (2004), pp. 2222–2233.
- [39] J. MAKHOUL, *Linear prediction: A tutorial review*, Proc. IEEE, 63 (1975), pp. 561–580.
- [40] S. MALLAT, *A Wavelet Tour of Signal Processing, Third Edition: The Sparse Way*, Academic Press, 3 ed., 2008.

- [41] K. S. R. MURTHY AND B. YEGNANARAYANA, *Epoch extraction from speech signals*, IEEE Trans. Audio, Speech, Lang. Process., 16 (2008), pp. 1602–1613.
- [42] E. PANTIN, J.-L. STARCK, AND F. MURTAGH, *Deconvolution and blind deconvolution in astronomy*, in *Blind Image Deconvolution: Theory and Applications*, CRC press, 2007, pp. 100–138.
- [43] D. PERRONE AND P. FAVARO, *A clearer picture of total variation blind deconvolution*, IEEE Trans. Pattern Anal. Machine Intelligence, 38 (2016), pp. 1041–1055.
- [44] L. R. RABINER, M. J. CHENG, A. E. ROSENBERG, AND C. A. MCGONEGAL, *A comparative performance study of several pitch detection algorithms*, IEEE Trans. Acoust., Speech, Signal Process., 24 (1976), pp. 399–418.
- [45] L. R. RABINER AND R. W. SCHAFER, *Theory and Applications of Digital Speech Processing*, Prentice-Hall Inc., 2011.
- [46] B. D. RAO AND K. KREUTZ-DELGADO, *An affine scaling methodology for best basis selection*, IEEE Trans. Signal Process., 47 (1999), pp. 187–200.
- [47] A. REPETTI, M. Q. PHAM, L. DUVAL, E. CHOUZENOUX, AND J. C. PESQUET, *Euclid in a taxicab: Sparse blind deconvolution with smoothed ℓ_1/ℓ_2 regularization*, IEEE Signal Process. Lett., 22 (2015), pp. 539–543, <https://arxiv.org/abs/1407.5465>.
- [48] I. W. SELESNICK, *Sparse deconvolution (an MM algorithm)*. <http://cnx.org/contents/f2738de6-b36d-458d-a2dd-2b50f375fe55@5/Sparse-Deconvolution-An-MM-Alg>.
- [49] I. W. SELESNICK AND I. BAYRAM, *Sparse signal estimation by maximally sparse convex optimization*, IEEE Trans. Signal Process., 62 (2014), pp. 1078–1092.
- [50] Q. SHAN, J. JIA, AND A. AGARWALA, *High-quality motion deblurring from a single image*, in *ACM Trans. Graphics*, vol. 27, ACM, 2008, p. 73.
- [51] R. R. SHENOY AND C. S. SEELAMANTULA, *Spectral zero-crossings: Localization properties and applications*, IEEE Trans. Signal Process., 63 (2015), pp. 3177–3190.
- [52] A. SMALL AND S. STAHLHEBER, *Fluorophore localization algorithms for super-resolution microscopy*, Nature Methods, 11 (2014), pp. 267–279.
- [53] A. TAKAHATA, E. NADALIN, R. FERRARI, L. DUARTE, R. SUYAMA, R. LOPES, J. ROMANO, AND M. TYGEL, *Unsupervised processing of geophysical signals: A review of some key aspects of blind deconvolution and blind source separation*, IEEE Signal Process. Mag., 29 (2012), pp. 27–35.
- [54] R. TIBSHIRANI, *Regression shrinkage and selection via the lasso*, J. Roy. Stat. Soc., Series B, 58 (1994), pp. 267–288.
- [55] A. N. TIKHONOV, V. I. ARSEININ, AND F. JOHN, *Solutions of Ill-posed Problems*, vol. 14, Winston Washington, DC, 1977.
- [56] F. ŠROUBEK AND P. MILANFAR, *Robust multichannel blind deconvolution via fast alternating minimization*, IEEE Trans. Image Process., 21 (2012), pp. 1687–1700.
- [57] D. WIPF AND H. ZHANG, *Revisiting Bayesian blind deconvolution*, J. Machine Learning Research, 15 (2014), pp. 3595–3634.
- [58] H. ZHANG, D. WIPF, AND Y. ZHANG, *Multi-observation blind deconvolution with an adaptive sparse prior*, IEEE Trans. Pattern Analysis and Machine Intelligence., 36 (2014), pp. 1628–1643.